Keystone engineering enables collective range expansion in microbial communities

Emrah Şimşek[1,2], César A. Villalobos[1,2,9], Kinshuk Sahu[1,2,9], Zhengqing Zhou[1,2], Nan Luo[1,8], Dongheon Lee[1,2], Helena R. Ma[1,2], Deverick J. Anderson[5,6], Charlotte T. Lee[2,7], and Lingchong You[1,2,3,4*]

[1]Department of Biomedical Engineering, Duke University, Durham, NC, 27708

[2]Center for Quantitative Biodesign, Duke University, Durham, NC, 27708

[3]Center for Genomic and Computational Biology, Duke University, Durham, NC, 27708

[4]Department of Molecular Genetics and Microbiology, Duke University School of Medicine, Durham, NC, 27708

[5]Division of Infectious Diseases, Department of Medicine, Duke University School of Medicine, Durham, NC, USA

[6]Duke Center for Antimicrobial Stewardship and Infection Prevention, Duke University School of Medicine, Durham, NC, USA

[7]Department of Biology, Duke University, Durham, NC, 27708

[8]Present address: Shenzhen Institutes of Advanced Technology, Chinese Academy of Sciences, Shenzhen 518055,
China

[9]These two authors contributed equally.

[*]Corresponding author. Department of Biomedical Engineering, Duke University, CIEMAS 1381, 101 Science Drive, Box 3382, Durham, NC 27708, USA.

Tel.: +1 (919)660-8408; Fax: +1 (919)668-0795; E-mail: you@duke.edu

Abstract

Keystone engineers profoundly influence microbial communities by altering their shared environment, often by modifying key resources. Here, we show that in an antibiotic-treated microbial community, bacterial spread is controlled by keystone engineering affecting dispersal—an effect hidden in well-mixed environments. Focusing on two pathogens, non-motile *Klebsiella pneumoniae* and motile *Pseudomonas aeruginosa*, we found that both tolerate a β-lactam antibiotic, with *Pseudomonas* being more resilient and dominating in well-mixed cultures. During range expansion, however, the antibiotic inhibits *Pseudomonas*' ability to spread unless it is near *Klebsiella*— *Klebsiella* degrades the antibiotic to create a "clear zone" that allows *Pseudomonas* to expand, at the expense of *Klebsiella*'s own growth, thus acting as a keystone engineer. As *Pseudomonas* spreads, it suppresses *Klebsiella* through resource competition. Our modeling and experimental analyses reveal that this keystone effect operates at a millimeter scale. We also observed similar keystone engineering by a *Bacillus* species isolated from a hospital sink, in both pairwise and eight-member bacterial communities with its co-isolates. These findings suggest that spatially explicit experiments are essential to understand certain keystone engineering mechanisms and have implications for surface-associated microbial communities like biofilms, as well as for diagnosing and treating polymicrobial infections involving drug-degrading, non-motile (e.g., *Klebsiella*), and drug-tolerant, motile (e.g., *Pseudomonas*) bacteria.

Introduction

A keystone species has a disproportionally large impact on its community relative to its abundance[1,2]. For example, removing the sea star *Pisaster ochraceous* drastically reduces biodiversity in its ecosystem because it allows mussel, its prey, to overgrow[1]. An ecosystem engineer affects other species in its community by modifying their environment. For example, beavers shape freshwater habitats that benefit many other species[3,4]. A species that meets both definitions is called a *keystone engineer*[5].

In microbial communities, keystone engineers are critical for maintaining biodiversity[6] and community functioning[7-10], including their impact on human health[11-14] (Though some of the given and following examples did not use the terms “keystone” and/or “engineer”, they describe mechanisms that align with the notion of keystone engineering). Microbial keystone engineers often play their role by breaking down complex resources into products utilizable by other microbes[11,14-19]. This role can also entail changing the environmental pH[19] or modulating the host immune response[12,13,20,21]. For instance, despite its low abundance, *Porphyromonas gingivalis* acts as a keystone that promotes overgrowth of the oral microbiota, which can cause inflammation[13].

Whether a microbe is a keystone engineer depends on context. For instance, in a synthetic mouse gut microbiota, *Bacteroides caecimuris* serves as a keystone engineer only when the polysaccharide inulin is the carbohydrate source[19], as *B. caecimuris* inhibits the growth of other species by acidifying the culture through inulin fermentation[19]. Likewise, *Bacteroides uniformis* can benefit or compete with butyrate-producing gut bacteria depending on the available carbohydrate sources[18].

While previous studies on keystone engineering have focused predominantly on growth or community structure[11-21], spatial structure is a ubiquitous environmental context for microbes. Many microbes live in spatially structured communities, such as biofilms[22-24]. In such an environment, survival depends on both mobility and effectiveness in nutrient utilization[25-28]. The mobility can be intrinsic or through interactions with other community members. For example, *Escherichia coli* can be transported by *Peanibacillus vortex*[29], and *Pseudomonas aeruginosa* cells hitchhike on shared biosurfactants[30,31]. Biosurfactant production enables collective spatial expansion (called swarming) but comes at a significant growth cost, and cheater cells that don't produce biosurfactants can destabilize this strategy during a prolonged spatial expansion of a

population[31]. These examples underscore the critical need for spatially explicit experiments to uncover microbial interactions. However, due to the lack of such well-controlled experiments, keystone engineering in the context of spatial expansion has not been demonstrated before.

Here, combining mathematical modeling and experiments, we reveal that in a microbial community treated with a β-lactam antibiotic, an immotile species acts as a keystone engineer enabling the spatial expansion of a motile species when sufficiently close. The immotile species detoxifies the environment by degrading the antibiotic, which would otherwise suppress the dispersal—but not the growth—of the motile species. This enables the motile species to expand, ultimately suppressing the growth of the immotile species and reducing it to a minority, consistent with a keystone role.

We demonstrated this keystone engineering in two pairwise communities: 1) clinical isolates of β-lactamase (Bla)-producing *Klebsiella pneumoniae* (*Klebsiella*) as the keystone engineer and *Pseudomonas aeruginosa* (*Pseudomonas*) as the motile species under cefotaxime (CTX) treatment, and 2) a nonpathogenic *Bacillus paranthracis* (Bp) with Bla genes as the keystone engineer and another, motile *Pseudomonas* strain (Pa22), co-isolated from the same hospital sink, under carbenicillin (CB) treatment. Finally, we demonstrated the applicability of Bp's keystone engineering on Pa22 in a synthetic community with six additional isolates from the same sink sample.

Our results suggest that a pathogen found responsible for a β-lactam resistant infection could test negative for Bla and/or β-lactam degradation (i.e., *Pseudomonas*), potentially yielding misleading diagnoses. Furthermore, our findings have broad implications for biofilm growth in mixed communities of pathogenic and nonpathogenic microbes in natural environments, such as hospital sinks.

Results

Klebsiella enabled *Pseudomonas* range expansion under β-lactam treatment at its own expense.

We tested the effect of a β-lactam antibiotic (CTX) treatment on the growth (i.e., biomass production) of *Pseudomonas aeruginosa* PA14 (*Pseudomonas*) and a Bla-producing clinical isolate of *Klebsiella pneumoniae* (*Klebsiella*)[32] in well-mixed liquid cultures. Both *Pseudomonas* and *Klebsiella* are prevalent pathogens in many common infection types[33,34] (**Supplementary**

Figure 1), suggesting that they have a strong niche overlap, making their community experiments clinically and ecologically relevant. We first grew *Klebsiella* and *Pseudomonas* in well-mixed pure cultures without or with CTX (2.5 μg/ml) (**Figure 1**A). Both species tolerated the CTX treatment, which reduced the biomass production of *Klebsiella* and *Pseudomonas* by 46% and 26%, respectively, when measured after 27 h (**Figure 1**A, bottom). *Klebsiella* grew ~ 1.3-times faster than *Pseudomonas* without antibiotics (during the first 6 h) (**Figure 1**A, top). With the CTX treatment, *Klebsiella* growth became detectable only after ~ 11 h of incubation (**Figure 1**A, bottom), while *Pseudomonas* growth was virtually unaffected (**Figure 1**A).

The results above show that *Klebsiella* grew faster without antibiotic treatment, whereas *Pseudomonas* grew faster under the CTX treatment. If the two species primarily interact through resource competition in well-mixed cocultures, we expect the dominance of *Klebsiella* without the CTX treatment and the dominance of *Pseudomonas* with the CTX treatment. To this end, we tested the growth of mix cultures, each starting with equal fractions of *Klebsiella* and *Pseudomonas*, with or without CTX treatment. Indeed, without CTX treatment, *Klebsiella* reached a relative abundance of 75.0% after 27 h (**Figure 1**B, top). With CTX (2.5 μg/ml) treatment, *Pseudomonas* reached a relative abundance of 99.9% after 27 h (**Figure 1**B, bottom).

We then examined the two species and their interactions on an agar surface where *Pseudomonas* could exhibit swarming motility[35]. We tested the effect of the β-lactam antibiotic CTX (2.5 μg/ml) on pure cultures of *Pseudomonas* or *Klebsiella* by inoculating them on agar and measuring their colonized areas and biomasses after 24 h of incubation (**Figure 1**C; **Supplementary Figure 2**, **Supplementary Figure 3**A). The CTX treatment suppressed *Pseudomonas* growth by 28-fold when measured by colony areas (**Figure 1**C; **Supplementary Figure 2**), or 22-fold when measured by biomass (**Supplementary Figure 3**A). This result is consistent with the studies that showed that *Pseudomonas*' swarming is inhibited by antibiotic treatment[36,37]. In contrast, the CTX treatment did not significantly affect *Klebsiella* colony growth (**Figure 1**C; **Supplementary Figure 2**). In both cases, *Klebsiella* colonies were smaller than those of *Pseudomonas* colonies (**Figure 1**C; **Supplementary Figure 2**).

We next measured the growth of a coculture starting with equal biomasses of the two species under the CTX treatment. The coculture colonized a 7.4-fold larger area and produced 6.2-fold greater biomass compared to *Pseudomonas* alone (**Figure 1**C; **Supplementary Figure 2**; **Supplementary Figure 3**A). Without antibiotic treatment, *Pseudomonas* alone grew better

than a mixture (**Figure 1**C; **Supplementary Figure 2**; **Supplementary Figure 3**A), though the difference was statistically insignificant (*p*–values are 0.081 and 0.25 for colonized area and biomass, respectively).

When mixed colonies were harvested and the relative abundances of the two species were measured based on their colony forming unit (CFU) morphologies (**Supplementary Figure 3**B), we found that *Pseudomonas* dominated in cocultures with (99.7%) or without (99.9%) CTX treatment (**Figure 1**C). Distributing the biomass in the mixed colonies with respect to these relative abundances, we found that *Klebsiella* always suffered from the mixed inoculation, while *Pseudomonas* benefited from it under the CTX treatment (**Supplementary Figure 3**A, compare the colored bars with and without a grey frame).

To facilitate the analysis of the colony composition in a spatially resolved manner, we used fluorescence proteins to label the two species (*Pseudomonas*-YFP and *Klebsiella*-mCherry). In a coculture consisting of these two labeled strains, we observed that *Klebsiella* was mostly confined at the seeding position, whereas the expanded colony front largely consisted of *Pseudomonas* (**Supplementary Figure 4**).

Collectively, our results indicate that the CTX treatment suppressed *Pseudomonas*' spatial expansion, which was rescued by *Klebsiella* in a co-culture (**Figure 1**C-D). In turn, the activated expansion of *Pseudomonas* suppressed the growth of *Klebsiella* (**Figure 1**D; **Supplementary Figure 3**A), which could be explained by a greater tolerance of *Pseudomonas* to CTX than *Klebsiella* (**Figure 1**A).

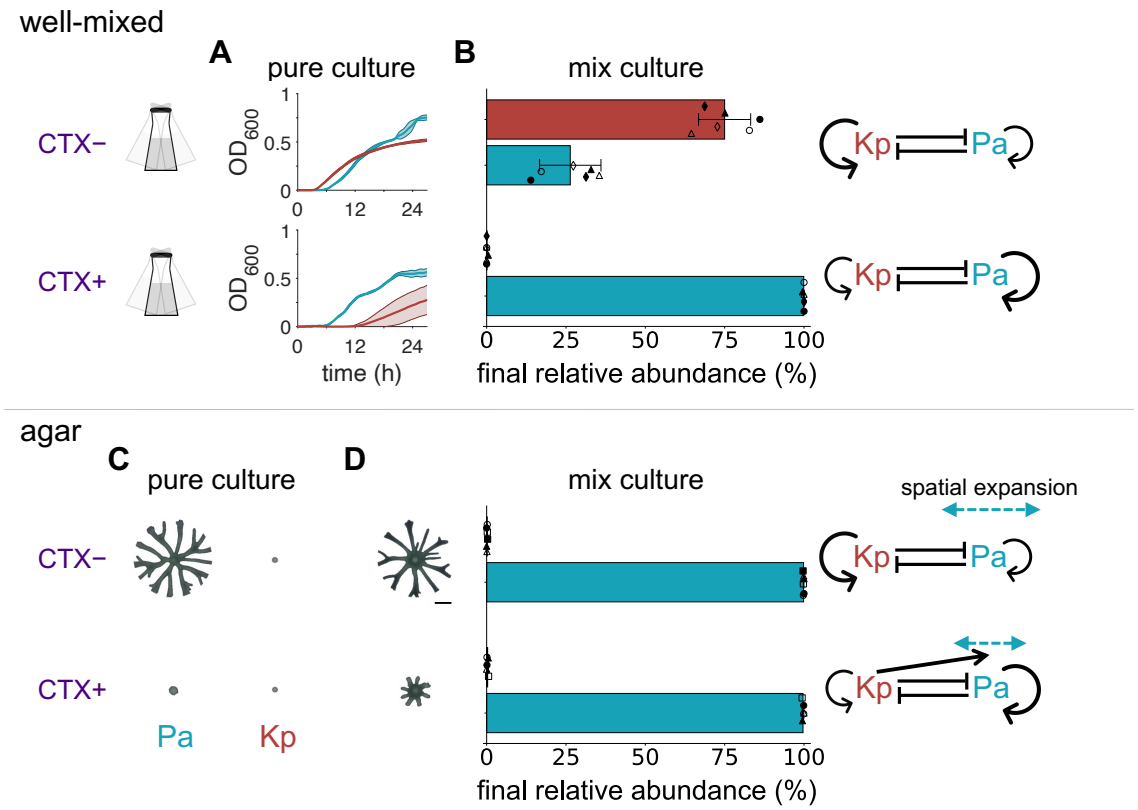

Figure 1: *Klebsiella* and *Pseudomonas* exhibited collective range expansion under CTX treatment at the cost of *Klebsiella*'s growth. *Klebsiella* and *Pseudomonas* pure cultures were grown overnight in Luria-Bertani (LB) broth. The cultures were then centrifuged, and the resulting cell pellets were resuspended in phosphate-buffered saline (PBS) supplemented with 8 g/l of casamino acids (see Methods). Kp: *Klebsiella*, Pa: *Pseudomonas*.

A. ***Pseudomonas* tolerated CTX treatment better than *Klebsiella*.** *Well-mixed* pure cultures of *Klebsiella* (dark red) and *Pseudomonas* (cyan) were inoculated at an initial OD_{600} = ~ 2.1×10^{-5}, and without or with CTX (2.5 μg/ml) (top and bottom, respectively). Curves and shades represent the average and the standard deviation, respectively, from two biological replicates each with three technical replicates. See Methods for details.

B. ***Pseudomonas* dominated *Klebsiella* under the CTX treatment in well-mixed co-cultures, which can be explained by resource competition.** Experiments were performed similarly to that in **Figure 1**A. The liquid growth media was inoculated with a 1:1 volume mixture of the two species at an initial OD_{600} = ~ 2.1×10^{-5}. Co-cultures were incubated for 27 h and then harvested to measure relative abundances by plating

(**Supplementary Figure 3**B). Circles, triangles, and diamonds represent independent replicates whose technical replicates were shown by solid or open markers. Data represented by diamonds were obtained using fluorescently labeled strains (*Pseudomonas*-YFP and *Klebsiella*-mCherry). Data and error bars represent the mean and the standard deviation from the independent experiments after their technical replicates were averaged.

C. ***Pseudomonas* range expansion was suppressed by CTX and rescued by *Klebsiella*.** 20 ml of swarming agar (0.55 %) media surface was center inoculated with 1 μl of a 1:1 volume mixture of *Klebsiella* and *Pseudomonas* (OD_{600} = ~ 0.43). Colony images were captured at 24 h, processed, analyzed for colony areas using a custom Python script (Methods; **Supplementary Figure 2**). See **Supplementary Figure 5** for raw images. Scale bar is 15 mm and for all the images shown.

D. **The rescue of the coculture range expansion occurred at the expense of *Klebsiella*'s growth.** After being imaged at 24 h, whole colonies were harvested by flooding with 5 ml of saline. The relative abundances of the two species in the harvests were estimated based on their distinct CFU morphologies (**Supplementary Figure 3**B). Circles, triangles, and squares show independent experiments, for which the solid and open markers represent technical replicates. The data and error bars represent the mean and the standard deviation from the independent experiments after their technical replicates were averaged. See **Supplementary Figure 3**A for the total biomasses of the cell harvests as well as its distribution between *Klebsiella* and *Pseudomonas*, estimated based on their relative abundances.

The rescuing by *Klebsiella* was likely due to its ability to produce Bla, which degrades CTX[32]. To test this notion, we collected supernatants from the *Klebsiella* pure cultures at ~ 6.3 h or media without cell inoculation as unconditioned control. After filter sterilizing the supernatants, we tested whether CTX-sensitive *Escherichia coli* could grow in them (**Supplementary Figure 6**A, top). Following 21 h of incubation, *E.* coli exhibited detectable growth in the *Klebsiella*-supernatant but not in the unconditioned control, consistent with the CTX degradation by *Klebsiella*-produced Bla[32] (**Supplementary Figure 6**A, bottom; see **Supplementary Figure 6**B, top for *Klebsiella* growth curves with the initial cell density of OD_{600} = ~ 5×10^{-4}, which was used for this experiment).

CTX suppressed *Pseudomonas*' spatial expansion in a dose-dependent manner.

We next measured the suppression of *Pseudomonas* spatial expansion (in terms of colonized area) using varied initial does of CTX (0 to 2.5 μg/ml) (**Supplementary Figure 7**). The suppression increased with the initial CTX dose (A_0), approximately following a Hill inhibition function.

Pseudomonas growth was virtually unaffected by CTX (2.5 μg/ml) treatment (**Figure 1**A). Thus, the suppression in *Pseudomonas*' spatial expansion (**Figure 1**C; **Supplementary Figure 7**) was likely due to the loss of motility and correlated with filamentous cell morphology (**Supplementary Figure 8**), consistent with previous reports that associating β-lactam-induced cell filamentation with reduced motility[38,39]. The extent of the filamentation of *Pseudomonas* cells was reduced when inoculated in a mixture with *Klebsiella* (**Supplementary Figure 8**), which restored *Pseudomonas*' spatial expansion (**Figure 1**D). A similar filamentation of *Pseudomonas* was observed in well-mixed liquid cultures under CTX (2.5 μg/ml) treatment, with or without *Klebsiella* (**Supplementary Figure 9**).

Theory reveals key determinants of the keystone engineering effect.

We conducted theoretical analysis to gain insight into the *Klebsiella*-mediated collective range expansion during antibiotic treatment. We assumed that the *Klebsiella* population leads to an antibiotic 'sink' and the growth media serves as a source for antibiotics (**Figure 2**A, top)[40]. We described the dependence of the effective spatial expansion ability (*M*) of *Pseudomonas* on the antibiotic concentration using the experimentally determined Hill function (**Supplementary Figure 7**). Solving the system assuming spherical symmetry (see Methods for details), we have:

$$M = \frac{1}{1+{a_0}^h\left(1-\frac{R}{d}\right)^h} \qquad (1)$$

where d defines the distance of *Pseudomonas* from the "sink" boundary (R) created by the *Klebsiella* population, a_0 is the initial antibiotic concentration normalized by its value for the half-maximum of *Pseudomonas*' effective spatial expansion ability ($a_0 = \frac{A_0}{A_C}$; see **Supplementary Figure 7** caption for A_C and h).

For a constant d, M decreases from 1 and approaches 0 with increasing a_0. For a given a_0, M decreases with increasing *d* (**Figure 2**A, bottom panel). For a sufficiently large a_0,

Pseudomonas' effective spatial expansion ability is only activated when $d < L_K$, where L_K denotes the distance at which M is half-maximum. Thus, L_K is a measure of the spatial scale of keystone engineering. For constant a_0, we predict L_K to increase with R (Supplementary Information, Equation S4), which we anticipated to have a weak dependence on *Klebsiella* seeding cell density (Supplementary Information, Equation S8). Critically, L_K can be substantially larger than R, indicating a long-range interaction (**Figure 2**A, bottom panel, $L_K = 2R$ for $a_0 = 2$).

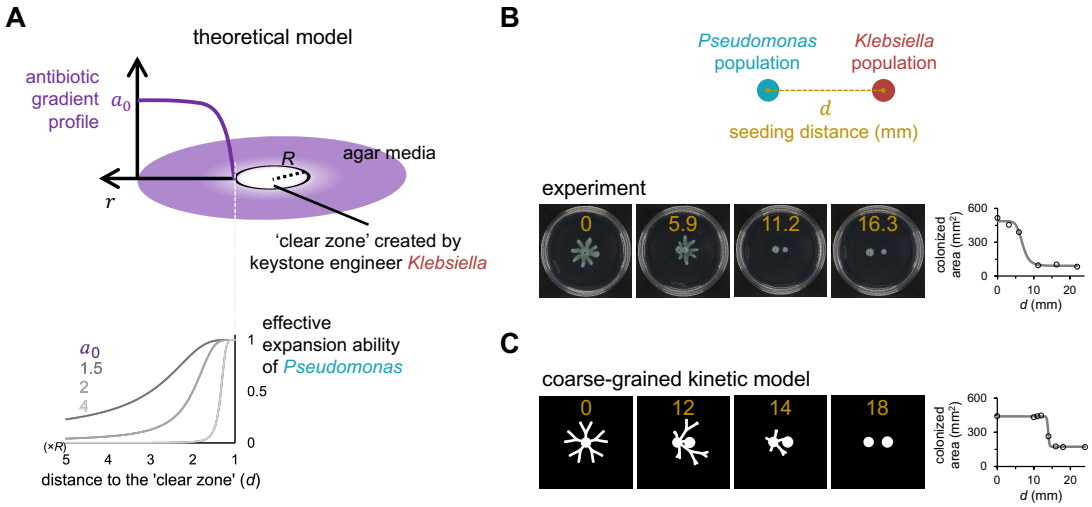

Figure 2: Spatial scale of the keystone engineering role.

A. **Theoretical model:**

***Top*: '*Klebsiella*–antibiotic' interaction**. Antibiotic concentration (a) has a steady-state gradient, under the assumption that a population of the keystone engineer *Klebsiella* acts as an antibiotic sink and the growth media serves as an antibiotic source. a is smaller when closer to the 'sink', where the antibiotic concentration is minimized at an ineffective value (see Supplementary Information for detailed analysis).

***Bottom*: '*Klebsiella*-antibiotic-*Pseudomonas*' interactions.** Equation 1 predicts that *Pseudomonas*' effective spatial expansion ability (M) is determined by its distance to the sink boundary (d) and the initial antibiotic concentration (a_0).

B. **Experiments corroborated the dependence of *Pseudomonas*' effective spatial expansion ability on its distance to *Klebsiella*.** The experiment in **Figure 1**C with CTX (2.5 μg/ml) was repeated with the only difference being 1 μl from the *Pseudomonas* (left) and 1 μl from the *Klebsiella* (right) cell suspensions were

inoculated side-by-side with various distance between them (gold in mm). The dishes were imaged at 23 h. The colonized areas were measured using a custom Python script and manually corrected using ImageJ when needed. The data was fitted to a Hill inhibition function (solid curve), where the Hill coefficient and the spatial scale of the keystone engineering (L_K) are 7.62 and 6.90 mm, respectively (R^2= 0.990). Each population initially occupied a circular area with a radius of ~1.5 mm. See **Supplementary Figure 10** for the raw data from all replicates and **Supplementary Figure 11** for the data from an experiment with the fluorescently labeled strains. Note that the half-maximum suppressing CTX dose was 1.29 μg/ml (**Supplementary Figure 7**).

C. **A coarse-grained kinetic model recapitulated the experimental range expansion patterns.** The results from the coarse-grained simulation at 48 h. *Left*. Black and white indicates bacteria are absent and present, respectively. *Right*. Total area where bacteria present was calculated using a custom MATLAB script and plotted as colonized area as a function of the seeding distance (center-to-center) between the *Pseudomonas* and *Klebsiella* populations (gold in mm). The data was again approximated by a Hill inhibition function (solid curve), where the Hill coefficient and L_K are 92.4 and 13.9 mm, respectively (R^2= 0.999). Each population initially occupied a circular area with a radius of 5 mm. See **Supplementary Figure 12** for the data at different time points.

Experiments corroborated the theoretical predictions.

To test Equation 1, we inoculated one *Klebsiella* population and one *Pseudomonas* population at varied distance (d) under CTX (2.5 μg/ml) treatment. Then, we quantified the range expansion as the colonized areas at 23 h, observing a sharp change at a certain distance value (**Figure 2**B), consistent with the prediction of the spatial scale of the keystone engineering (L_K) above. The range expansion had a bias towards the *Klebsiella* population, which we confirmed by repeating this experiment with the fluorescently labeled strains (**Supplementary Figure 11**). We demonstrated the robustness of the existence of L_K, repeating the same experiment, also with varied *Klebsiella* seeding cell density (**Supplementary Figure 10**).

A coarse-grained kinetic model recapitulated the experimental range expansion patterns.

The spatial patterns of the range expansion (**Figure 2**B) were not considered in our theoretical estimation of M and L_K above. The spatial patterns are anticipated to be a function of not only the antibiotic gradient and the *Pseudomonas*' spatial expansion ability the latter determines but also the spatiotemporal dynamics of the abundances of the species and nutrients. Thus, we next accounted for these factors and built a coarse-grained model, enabling a more constrained simulation of spatial expansion dynamics (Methods and **Supplementary Table 2**).

This model builds upon our previous models for *Pseudomonas* branching[41] and Bla-mediated population dynamics in response to β-lactam treatment[32] (see Methods). We simulated the range-expansion dynamics with varied seeding distance (d) between one *Klebsiella* population and one *Pseudomonas* population. Again, we quantified the total colonized area (at 48 h; see **Supplementary Figure 12** for different time points) and found a sharp onset of range expansion as d decreased below a critical value, consistent with the existence L_K (**Figure 2**C).

The keystone engineering occurred in a pairwise community of hospital sink co-isolates, *Bacillus paranthracis* and *Pseudomonas aeruginosa*.

Colonization of hospital sink drains (e.g., p-traps) has been associated with pathogens such as *K. pneumoniae*[42] and *P. aeruginosa*[43]. Moreover, biofilms formed in the p-traps of connected sinks and expanded upwards 2.5 cm/day, possibly due to surface-associated bacterial motility[44]. If sufficiently close to the sink strainer, running sink water can lead to the spread of bacteria to the environment[44], posing a health risk.

We next tested whether the keystone engineering could occur in communities of bacteria isolated from the same sink p-trap at Duke University Hospital. Two isolates, 192621 and 192622, were identified by 16S rDNA sequencing as *Bacillus paranthracis* and *P. aeruginosa*, respectively.

We first tested the effect of carbenicillin (CB; 10 μg/ml) treatment on the growth of the two isolates. Specifically, we grew *B. paranthracis* 192621 (Bp) and *P. aeruginosa* 192622 (Pa22) in pure liquid cultures without or with CB (10 μg/ml) (**Figure 3**A). Both species tolerated the CB treatment, but Pa22 grew faster than Bp under both conditions. If the two species primarily interact through resource competition in well-mixed cocultures, we expect the dominance of Pa22 under both conditions. To this end, we tested the growth of mix cultures, each starting with equal

fractions of Bp and Pa22, with or without CB treatment. Indeed, Pa22 dominated after 27 h for both cases, where Bp was undetectable (< 0.1%) (**Figure 3**B).

When tested on agar, however, only a mixture of Bp and Pa22 exhibited spatial expansion after 24 h under treatment by CB (10 μg/ml; ~ 2.4-times the concentration for the half-maximum suppression of the spatial expansion of Pa22 when alone, **Supplementary Figure 13**). While mixing Pa22 with Bp promoted biomass production under the CB treatment by 4-fold, Bp itself became undetectable (< 0.1%) in the final population (**Figure 3**D; see **Supplementary Figure 14**A for biomass data). Supernatants from CB-treated pure cultures of Bp allowed the growth of CB-sensitive *E. coli* (**Supplementary Figure 15**), indicating the degradation of CB in the environment by Bp. These results suggest that Bp served the keystone engineer role on Pa22 only during community spatial expansion.

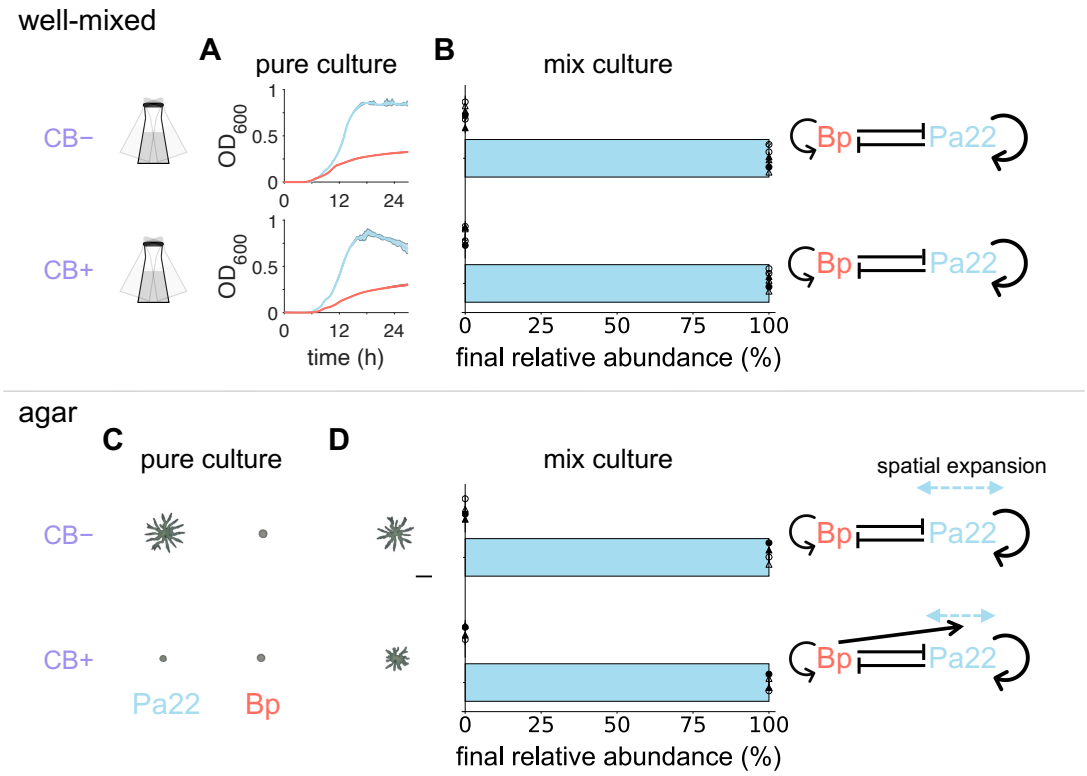

Figure 3: The keystone engineering in a pairwise community of hospital sink isolates, Bp and Pa22. Bp and Pa22 pure cultures were grown overnight in LB broth. The cultures were then centrifuged, and the resulting cell pellets were resuspended in PBS

supplemented with 8 g/l of casamino acids (see Methods). Bp: *Bacillus paranthracis*, Pa22: *Pseudomonas aeruginosa* 192622.

A. **Pa22 tolerated CB treatment better than Bp.** *Well-mixed* cultures of Bp (red) and Pa22 (light blue) were inoculated, with the initial cell density of OD_{600} = ~ 2.1×10^{-5}, and without or with CB (10 μg/ml) (top and bottom, respectively). Curves and shades represent the average and the standard deviation, respectively, from two biological replicates each with three technical replicates.

B. **Pa22 dominated Bp in well-mixed cocultures via resource competition.** The liquid growth media was inoculated with a 1:1 volume mixture of the two species at the starting cell density of OD_{600} = ~ 2.1×10^{-5}. Co-cultures were incubated for 27 h and then harvested to measure relative abundances by plating (**Supplementary Figure 14**B). Circles and triangles represent independent replicates whose technical replicates were shown by solid, open, or lined markers. Data and error bars represent the mean and the standard deviation from the independent experiments after their technical replicates were averaged.

C. **Pa22's range expansion was suppressed by CB treatment and rescued by Bp.** 20 ml of agar (0.55 %) media surface was center inoculated with 1 μl of a 1:1 volume mixture of Bp and Pa22 with or without CB (10 μg/ml) at the initial cell density of OD_{600} = ~ 0.34 or ~ 0.43). Images of the colonies were captured at 24 h. The images were processed and analyzed for colonized areas using a custom Python script (Methods). See **Supplementary Figure 16** or all raw images. Scale bar is 15 mm and for all the images shown.

D. **The rescue of the coculture range expansion occurred at the expense of Bp's growth.** After being imaged at 24 h, whole colonies were harvested by flooding with 5 ml of saline. The total biomass was calculated by multiplying the absorbance (OD_{600}) and the volume of the suspension. Relative contributions of Bp and Pa22 to the total biomass of the mixture were determined by multiplying the total biomass with the relative abundances of the two species determined by plating, based on CFU morphologies (**Supplementary Figure 14**B). Circles (inoculum density of OD_{600} = ~ 0.43) and triangles (inoculum density of OD_{600} = ~ 0.34) represent independent experiments, for which the solid and open markers show technical replicates. Data and error bars show the mean and standard deviation, respectively, from all the replicates.

Keystone engineering occurred in a synthetic community of sink isolates

We next tested if Bp's keystone engineering on Pa22's spatial expansion could occur in the presence of other members of sink isolates. To this end, we assembled an 8-member community, which we termed "SynkC", by introducing six additional isolates from the same sink sample from which we isolated both Bp and Pa22. SynkC consisted of six distinct taxonomic groups based on 16S rDNA-based microbiome sequencing (see **Supplementary Figure 17** for the spatial growth phenotypes of the additional isolates, with or without the CB treatment).

We ran agar experiments with SynkC with equal starting biomasses of all the eight members or by leaving out Bp (SynkC-Bp). Again, spatial expansion under the CB treatment occurred only when Bp was included (**Figure 4**, images), though Bp was not detected in the final population of SynkC (**Figure 4**, pie charts). In addition to promoting the spatial expansion and a ~ 2.7-fold greater biomass production, the initial presence of Bp also led to a greater community diversity under the CB treatment (only Pa22 in the final SynkC-Bp vs. Pa22 and *Enterobacter sp*. in the final SynkC) (**Figure 4**, pie charts).

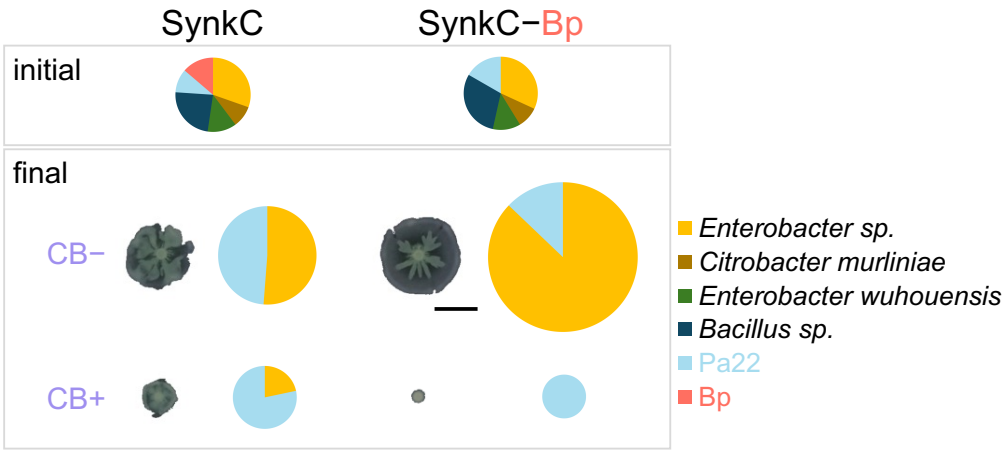

Figure 4: The keystone engineering in SynkC, an 8-member, synthetic community of hospital sink co-isolates.

The agar (0.55%) surface was inoculated with 1 μl of a mixture containing equal biomasses of all the eight isolates (SynkC) or all but Bp (SynkC–Bp) (OD_{600} = ~ 0.34). Images of the colonies were captured at 24 h. Then, whole colonies were harvested by flooding with ~ 5 ml of saline. The biomasses of the cell harvests were calculated by measuring the absorbance (OD_{600}) of each harvest suspension and multiplying it by the

suspension volume. The initial and final cell suspensions were stored as frozen glycerol stocks and underwent 16S microbiome sequencing to determine the initial and final relative abundances of different community members. Each of the pie charts above shows six groups, with the *Enterobacter sp.* and *Bacillus sp.* groups representing the combined abundance of two isolates each, while all other groups represent a single isolate. For the final time point, relative areas of the pie charts represent the distribution of the respective biomasses measured. Two independent experiments, each with technical replicates, yielded similar results. A representative set of data was shown here, after the images being processed using our custom Python script. CB (10 μg/ml) was used when applicable. See **Supplementary Figure 18** for the raw data. See **Supplementary Figure 17** for the identities and phenotypes of the individual isolates other than Bp and Pa22. Scale bar is 15 mm and for all the images shown.

Discussion

Our study provides a concrete demonstration that context—specifically spatial structure and chemical stress—can reveal a species' keystone engineer role. By degrading β-lactam antibiotics, an immotile Bla-producing species (*Klebsiella* or *Bacillus paranthracis*) creates a "clear zone" that restores the motility-based range expansion of a more resilient partner (*Pseudomonas*). Although the keystone engineer eventually becomes a minority due to resource competition, its transient facilitation is essential for spatial expansion and overall community success. This mechanism could contribute to the observed rapid biofilm formation in sink-associated microbial communities[44].

Our results broaden the canonical interpretation of keystone species, which typically emphasizes effects on growth or community structure[11-21]. Two contextual factors are critical for our system. One is spatial expansion, as mobility only matters in a spatially structured environment. This context-dependency is reminiscent of a recent example in which we show that the spatial expansion of *Pseudomonas* not only makes a cooperative trait essential[30] but also allows non-cooperating variants (so-called "cheaters") to leverage their growth advantage from the lack of cooperative trait expression, enabling them to outcompete the cooperating individuals[31]. The other contextual factor is antibiotic stress, which primarily suppresses mobility instead of the growth of *Pseudomonas*. Together, these factors shift the net effect of the keystone engineer from competitive to facilitative. This shift aligns with the stress gradient hypothesis,

which suggests that positive interactions dominate negative interactions in more stressful environments[45-48].

The principles uncovered here are likely generalizable. Other species or consortia could similarly modify their environment—through pH shifts[19], enzyme secretion[49,50], nutrient release/break-down[18,49,50], or other chemical changes—to unlock traits like motility[51,52], biofilm growth[53-55], or nutrient utilization (i.e., necrotrophy[49]) relevant only in spatially structured habitats. Such facilitation may be common in natural and engineered microbial communities but remain untapped due to a lack of spatially explicit experimental inquiry.

Clinically, our work suggests that certain Bla producers may play a crucial, even if transient, role in promoting the spread of more virulent pathogens, such as *Pseudomonas*, even if they remain undetected in standard assays. Current microbiome analyses often exclude low-abundance taxa[56], potentially missing these keystone engineers and underestimating their influence on infection dynamics.

In conclusion, recognizing the context-dependent emergence of keystone engineering enriches our understanding of microbial ecology, offers insights for controlling infections, and opens new avenues for studying hidden facilitators in complex microbial ecosystems.

Methods

Bacterial growth media and procedures

In every experiment, bacteria were first streaked on a Luria-Bertani (LB) agar plate from their frozen glycerol stock, and a single colony was incubated overnight in liquid LB media at 37 °C and 225 r.p.m.

For all experiments, PBS (2.4 g/l Na_2HPO_4 (anhydrous), 3 g/l KH_2PO_4 (anhydrous), 0.5 g/l NaCl, 1 mM $MgSO_4$, and 0.1 mM $CaCl_2$) supplemented with casamino acids (8 g/l, unless otherwise noted) was used. Agar (final concentration of 0.55 %) was used when applicable.

The media was prepared following a recipe adapted from Xavier *et al*.[57]: To make 1 liter of 5x phosphate buffer stock solution, 12 g Na_2HPO_4 (anhydrous), 15 g KH_2PO_4 (anhydrous), and 2.5 g NaCl were dissolved in deionized water and sterilized by autoclaving. The casamino acids

stock solutions were made at 20 % (w/v) by microwaving 40 g casamino acids (Gibco™ Bacto™ 223120) in deionized water, sterilized by filtering (0.22 μm) and stored at 4 °C. The main solutions of agar were made at 1.25 % (w/v) on the day of the experiment dissolving granulated agar (BD Difco™ 214530) in deionized water and sterilizing by autoclaving. Then, appropriate amounts were immediately used to prepare the experimental media.

In the experiments and overnight cultures with the *Pseudomonas*-YFP and *Klebsiella*-mCherry variants, gentamycin (15 μg/ml) was added for the maintenance of the plasmids. aTc (100 ng/ml) was also added for inducing the mCherry expression. All antibiotic solutions used in the study were made fresh on the day of the experiment.

All OD_{600} measurements were taken using 200 μl samples and a plate reader (Tecan Infinite 200).

Well-mixed liquid cultures

We grew 2-3 ml cells in 16 ml culture tubes at 37 °C and 225 r.p.m. The cultures with aTc were protected from light.

Growth curve experiments

We measured the growth curves of bacteria using a plate reader (Tecan Infinite 200). In each well of a 96-well plate, we added 195 μl liquid media and 5 μl cell inoculum culture (prepared by centrifuging overnight-grown cells at 1150 g for 5 min and then resuspending in the liquid medium). To prevent evaporation, we used Nunc Edge multi-well plates (Thermo Scientific) with built-in water reservoirs. The cells were then incubated in the plate reader at 37 °C, and OD_{600} measurements were taken at 10 min intervals after the plate being shaken rigorously. For technical replicates of a particular condition, cells from the same inoculum were inoculated in different wells of a 96-well plate and measured. Background signals measured from media containing no cells were subtracted from the data. Custom MATLAB scripts were used for data analysis, during which a four time point moving average was applied to the raw OD_{600} time series data.

Agar media experiments

20 ml growth media was solidified in 100 mm petri dishes. Overnight-grown cells were centrifuged at 1150 g for 5 min and then resuspended in the liquid medium to prepare a cell

inoculum culture. The seeding droplet volume from cell inoculum cultures was 1 μl. The seeded plates were incubated at 37 °C, agar side up.

CTX/CB environmental degradation assays

The protocol used was adapted with minimal changes from our previous study[32]: Briefly, 3 ml liquid media with/without the keystone engineer bacteria (*Klebsiella* or Bp) inoculated (initial cell density of OD_{600} = ~ 5×10^{-4}) and with/without the antibiotic (2.5 μg/ml CTX or 10 μg/ml CB) addition were incubated at 37 °C and 225 r.p.m. At ~ 6.3 h, 1 ml samples from the media were removed, in which clavulanic acid (5 μg/ml final concentration) was then added to prevent any further Bla activity. Next, supernatants were prepared by filtration of these 1 ml samples using 0.22 μm cellulose acetate filters (VWR). Finally, the supernatants were inoculated with *E. coli* MC4100Z1 at initial cell density of OD_{600} = ~ 5×10^{-4}, at which the *E. coli* is sensitive to the antibiotic treatments here. Then, OD_{600} measurements were taken after 21 h incubation at 37 °C at 225 r.p.m.

Relative abundance measurements based on colony forming unit (CFU) morphology

As shown in **Supplementary Figure 3**B and **Supplementary Figure 14**B, CFUs were grown on LB agar (1.5 %) for 20 h at 37 °C to determine the relative abundance of the constituent species in pairwise mixed cultures. To do so, cell harvests were serially diluted in sterile saline (11.6 g/l NaCl) solution down to ~ 100 CFUs per 100 μl spread on a 100-mm LB agar plate.

Bacterial strains

P. aeruginosa PA14 (*Pseudomonas*), a clinical *K. pneumoniae* isolate D-005 from Deverick J. Anderson's laboratory (*Klebsiella*), *E. coli* MC4100Z1, and the hospital sink p-trap isolates described below were used. For some experiments variant strains that expressed spectrally distinct fluorescent proteins from a plasmid, *Pseudomonas*-YFP[31] and *Klebsiella*-mCherry (this study, see Methods and **Supplementary Table 1**), were used.

Construction of the Klebsiella-mCherry strain

<u>Strain & transformation</u>

Zymo Mix & Go Transformation kit (Zymo Research) was used to make *K. pneumoniae* D-005 chemically competent with one modification: the overnight culture of D-005 was re-grown in super optimal broth (SOB) supplemented by 0.7 mM (final concentration) ethylenediaminetetraacetic acid (EDTA)[58].

Plasmid construction

ptetmCherryGMR was constructed from the parent plasmids ptetmCherry[59], pUCP30T-eCFP plasmid[60], and pJ1996_v2[61]. The ptetmCherry plasmid without the chloramphenicol resistance gene, the gentamicin resistance gene, and a DNA fragment containing two transcription terminators were PCR amplified from the ptetmCherry, pUCP30T-eCFP, and pJ1996_v2 plasmids, respectively, by DNA primers with overhangs. The resulting linear DNA fragments were digested by DpnI and subsequently column purified with DAN Clean & Concentor-5 (Zymo Research). Then, they were ligated together with NEBuilder HiFi DNA Assembly Master Mix (NEB #E2621) to yield the final plasmid. The final plasmid was transformed into Top10F' to propagate, miniprepared with Zymo Plasmid Miniprep-Classic kit (Zymo Research) and sequenced by Sanger sequencing (Genewiz/Azenta Life Sciences) to validate.

All the DNA primers were purchased from Integrated DNA Technologies and listed in **Supplementary Table 1**.

SynkC: Isolation of bacteria from the sink p-traps and their taxonomic identification

Strain ID	**Taxonomic unit ID in Figure 4, and Supplementary Figures 17-18**	**ID suggested by the Azenta pipeline**	**ID suggested by the SeqCenter pipeline**
ESY55	Pa22	*Pseudomonas aeruginosa* ATCC10145	*Pseudomonas aeruginosa*
ESY57	Bp	*Bacillus paranthracis* MCCC1A00395	*Bacillus*
ESY66	*Enterobacter wuhouensis*	*Enterobacter wuhouensis/ludwigii*	*Enterobacter cloacae*
ESY73	*Bacillus sp*.	*Bacillus aerophilus/stratosphericus/altitudinis*	*Bacillus sp*.
ESY80	*Citrobacter murliniae*	*Citrobacter murliniae / freundii*	*Citrobacter*
ESY83	*Enterobacter sp*.	*Enterobacter bugandensis* 247BMC	*Enterobacter*

ESY92	*Bacillus sp.*	*Bacillus aerophilus/stratosphericus/altitudinis*	*Bacillus sp.*
ESY93	*Enterobacter sp.*	*Enterobacter sichuanensis/asburiae*	*Enterobacter*

The members of SynkC were isolated by propagations of a sample collected from a sink p-trap in an intensive care unit in a recently constructed bedtower at the Duke University Hospital. Sterile tubing was fed down into the p-trap and a 50 ml syringe was used to agitate the fluid to collect biofilm portions and then withdraw a sample[62]. 50 µl of p-trap water was used to inoculate 950 µl of tryptic soy broth in a 2 ml deep well plate (Thermo Scientific) and grown for 16 h at 37 °C with shaking at 700 r.p.m. The resulting culture was glycerol stocked (25% glycerol) and frozen. In parallel, it was serially diluted to 10^{-6} in phosphate buffered saline and 10 µl of dilutions from 10^{-3} to 10^{-6} were plated on tryptic soy agar (TSA) with and without 100 µg/ml carbenicillin. The plates were incubated at 37 °C for 10 h and at room temperature for 66 h.

Pa22 (ESY55) and Bp (ESY57) were isolated via restreaking different parts of the resulting colonies on fresh agar plates and incubating for 18 h at 37 °C. A new set of overnight cultures were then made by inoculating 2 ml of tryptic soy broth with individual colonies on the restreaked plates and incubating for 16 hours at 37 °C. These cultures were then glycerol stocked as the eventual Pa22 and Bp. Subsequent colonies from these stocks were sent for 16S sequencing at Azenta Life Sciences for species identification.

ESY66 and ESY73 were isolated as follows: First, the glycerol stock of the original overnight culture described above was inoculated LB broth and then grown for ~ 8 h at 37 °C with shaking at 225 r.p.m. The resulting culture was glycerol stocked (25% glycerol) and frozen. This stock is called the “master stock” hereafter. The master stock was diluted ~ 10^4 -fold in 11.6 g/l saline, and 100 µl of the dilution was plated on TSA plates. The plates were incubated at 37 °C for ~ 20 h. Individual colonies were restreaked on LB agar plates, and the plates were incubated at 37 °C for ~ 20 h, again. Then, overnight cultures were grown by inoculating 2 ml of LB broth with individual colonies from the restreaked plates and incubating for ~ 18 h at 37 °C with shaking at 225 r.p.m. These cultures were then glycerol stocked as the eventual isolates used in **Figure 4**, **Supplementary Figure 17**, and **Supplementary Figure 18**. Individual colonies from these stocks were sent for 16S sequencing at Azenta Life Sciences for species identification.

ESY80, ESY83, ESY92, and ESY93 were isolated as follows: First, ~ 1 μl from the master stock was inoculated on swarming agar media and incubated for ~ 24 h at 37 °C. The final colony was suspended in 11.6 g/l saline and then glycerol (25 %) stocked and frozen. This new frozen stock was diluted ~ 10^5-fold in 11.6 g/l saline, and 100 μl of the dilution was plated on TSA plates. The plates were incubated at 37 °C for ~ 20 h. Individual colonies were restreaked on LB agar plates, and the plates were incubated at 37 °C for ~ 20 h, again. Then, overnight cultures were grown by inoculating 2 ml of LB broth with individual colonies from the restreaked plates and incubating for ~ 18 h at 37 °C with shaking at 225 r.p.m. These cultures were then glycerol stocked as the eventual isolates used in **Figure 4**, **Supplementary Figure 17**, and **Supplementary Figure 18**. Individual colonies from these stocks were sent for 16S sequencing at Azenta Life Sciences for species identification.

16S microbiome sequencing by SeqCenter

16S V3/V4 region sequencing (20000 reads) service of SeqCenter, LLC was used. Aliquots from cell harvests were supplemented by glycerol (25 % final concentration) before being frozen at -80 °C. The frozen aliquots were shipped overnight to the company's facility on dry ice.

DNA extraction

All standard DNA extractions at SeqCenter follow the ZymoBIOMICS™ DNA Miniprep Kit. 20 - 200 μl from the samples submitted were transferred into 550 μl of lysis solution. Cells suspended in lysis solution were transferred into the ZR BashingBead™ Lysis Tubes and mechanically lysed using the MP FastPrep-24™ lysis system with 1 min of lysis at maximum speed and 5 min of rest for 5 cycles. Samples were then centrifuged at 10000 g for 1 min. 400 μl of supernatant was transferred from the ZR BashingBead™ Lysis Tube to a Zymo-Spin™ III-F Filter and centrifuged at 8000 g for 1 min. 1200 μl of ZymoBIOMICS™ DNA Binding Buffer was added to the effluent and mixed via pipetting. 800 μl of this solution was transferred to a Zymo-Spin™ IICR Column and centrifuged at 10000 g for 1 min. This step was repeated until all material was loaded onto the Zymo-Spin™ IICR Column. DNA bound to the Zymo-Spin™ IICR Column was washed 3 times with 400 μl and 700 μl of ZymoBIOMICS™ DNA Wash Buffer 1 and then 200 μl of ZymoBIOMICS™ DNA Wash Buffer 2 with a 1-min spin down at 10000 g for each, respectively. Washed DNA was eluted using 75 μl of ZymoBIOMICS™ DNase/RNase Free Water following a 5-min incubation at room temperature and a 1-min spin down at 10000 g. The Zymo-Spin™ III-HRC Filter was prepared using 600 μl of the ZymoBIOMICS™ HRC Prep Solution and

a centrifugation at 8000 g for 3 min. Eluted DNA was then purified by running the effluent through the prepared Zymo-Spin™ III-HRC Filter. Final DNA concentrations were determined via Qubit.

Sequencing

Samples were prepared using Zymo Research's Quick-16S kit with phased primers targeting the V3/V4 regions of the 16S gene. The specific primer sequences are found below:

Amplified region	Forward sequence	Reverse sequence
V3/V4	341f CCTACGGGDGGCWGCAG CCTAYGGGGYGCWGCAG	806r GACTACNVGGGTMTCTAATCC

Following clean up and normalization, samples were sequenced on a P1 600cyc NextSeq2000 Flowcell to generate 2×301bp paired end (PE) reads. Quality control and adapter trimming was performed with bcl-convert (v4.2.4).

Analysis

Sequences were imported to Qiime21 for analysis. Primer sequences were removed using Qiime2's cutadapt2 plugin using the following degenerate primer queries:

Region	Forward trim sequence	Reverse trim sequence
V3/V4	CCTAYGGGNBGCWGCAG	GACTACNVGGGTMTCTAATCC

Sequences were then denoised using Qiime2's dada2 plugin3. Denoised sequences were assigned operational taxonomic units (OTUs) using the "Silva 138 99% OTUs full-length sequence database" and the VSEARCH4 utility within Qiime2's feature-classifier plugin. OTUs were then collapsed to their lowest taxonomic units, and their counts were converted to reflect their relative frequency within a sample.

Note that, for SynkC, neither the SeqCenter microbiome sequencing nor the Azenta Life Sciences 16S sequencing-based species identification pipelines could distinguish the members within the *Enterobacter sp*. and *Bacillus sp* taxonomic units. The identities of Pa22, Bp, *Citrobacter murliniae*, and *Enterobacter wuhouensis* were better resolved to species level from the best fits from the pipeline of Azenta Life Sciences, so we used those identities. We confirmed that these four isolates did not fall into either the *Enterobacter sp*. or the *Bacillus sp* taxonomic

units in the pipeline of SeqCenter, which was used to generate the relative abundance data in **Figure 4** and **Supplementary Figure 18**.

Imaging

Bacterial colonies on agar plates were imaged with a UVP Colony Doc-It Imaging Station with epi white light, using the same brightness and contrast settings for all images. The same z-plane focus was applied to all images within the same independent experiment.

Microscopic imaging was performed using a Keyence BZ-X710 microscope and Keyence BZX Software Suite 1.3.1.1. To image a whole swarming colony, its entire plate was scanned and imaged, and the resulting images were stitched using the built-in algorithm of the software.

Image analyses

A custom Python script was used for processing and analyzing the colonized area for bacterial colony images. This script firsts finds and removes the plate boundaries. Then, the bacterial colony (or colonies when applicable) is automatically segmented using a user-defined threshold intensity value. Finally, the image background is changed to plain white for display purposes. When applicable, the script calculated the seeding distance between different species as the Euclidean distance between two positions, defined by the user based on the distinct appearance of the inoculum zones. For each case, the segmentation results were manually validated and corrected using Image J manual tools when necessary.

Custom MATLAB scripts were used the coarse-grained kinetic model simulations and the corresponding analyses.

Coarse-grained kinetic model

"*Pseudomonas* cell density"

$$\frac{dP}{dt} = \frac{\int_{\Omega} \alpha_P G_P P dx}{WDRL}$$

"*Pseudomonas* branch extension"

$$\frac{dL}{dt} = \frac{\gamma}{WDR} \int_{\Omega} \alpha_P G_P P \frac{A_C^h}{A_C^h + A^h} dx$$

"*Klebsiella* cell density"

$$\frac{\partial E}{\partial t} = \alpha_P (G_E - L_E) E + D_E \nabla^2 E$$

"Nutrient concentration"	$$\frac{\partial N}{\partial t} = -\beta_N G_P P - \beta_{EN} G_E E + D_N \nabla^2 N$$
"Cefotaxime concentration"	$$\frac{\partial A}{\partial t} = -\kappa_B B A + D_A \nabla^2 A$$
"Extracellular Bla concentration"	$$\frac{\partial B}{\partial t} = \alpha_P L_E B_{in} E - d_B B + D_B \nabla^2 B$$
"*Pseudomonas* growth function"	$$G_P = \frac{N}{N + K_N} \frac{C_m}{C_m + P + E} \left(1 - \frac{P + E}{K_C}\right)$$
"*Klebsiella* growth function"	$$G_E = \mu_E G_P$$
"*Klebsiella* lysis function"	$$L_E = \phi_E G_E \frac{A^{h_2}}{A_E^{h_2} + A^{h_2}}$$

We have formulated the above mathematical model building upon our previous models for *Pseudomonas* branching pattern formation[41] and Bla-producing bacteria population dynamics under beta-lactam treatment[32]. The former one assumes that a *Pseudomonas* population splits the energy it derives from nutrients into cell growth and spatial expansion at a certain ratio. As it does so, nutrient gradients form around it. The *Pseudomonas* population expands in the increasing direction of these nutrient gradients, with a bias towards the steepest one. Eventually, *Pseudomonas* colonizes the surface by forming its characteristic branching patterns. Here, we modified this model to incorporate the suppression of *Pseudomonas*' effective spatial expansion ability by antibiotics. Furthermore, to account for the interspecies interactions, we weaved the model for Bla-producing bacteria population dynamics under beta-lactam treatment into this modified version of the *Pseudomonas*' swarming model.

We used the parameter values from the original papers[32,41], with some minor modifications, when possible. The diffusivities of the antibiotic and beta-lactamase were chosen based on their molecular weights relative to nutrients (i.e., casamino acids), as suggested by Einstein's relation. The parameter values for the CTX concentration for the half-maximum suppression of *Pseudomonas*' effective spatial expansion ability (A_C) and the sharpness of this

suppression (h) were used from the Hill-fits to our experimental data above (see **Supplementary Figure 7**A caption). We assumed no spontaneous degradation of the antibiotic or nutrient recycling after lysis. In addition to the diffusivities of the antibiotics and β-lactamases, another added parameter was the nutrient consumption rate of *Klebsiella* through cell growth. This parameter had to be constrained tightly as *Pseudomonas* would otherwise avoid *Klebsiella*-colonized territory due to nutrient depletion. Finally, we added another parameter to account for our experimental observation above that *Pseudomonas* spatial expansion is biased towards *Klebsiella* (**Figure 2**B and **Supplementary Figure 11**). This parameter essentially determines the relative dominance of *Pseudomonas*' range expansion on nutrient gradients versus antibiotic gradients depending on their global profiles: *Pseudomonas* would move towards decreasing antibiotic concentration (i.e., the *Klebsiella* neighborhood), except when $d = 0$, if the spatial global average of antibiotic concentration is greater than A_C and if the global minimum of nutrient concentration is greater than a factor (0.7 as the default value) of the nutrient concentration for half maximum specific growth rate. This constraint was not applied for $d = 0$.

The partial differential equations were numerically solved using a custom MATLAB implementation of the alternating direction implicit method by applying no-flux boundary conditions. See **Supplementary Table 2** for the definition and values of the model parameters as well as the initial conditions used.

Acknowledgments

We thank Lawrence A. David, Joanna B. Goldberg, David K. Karig, Jeffrey Letourneau, Jia Lu, Alice S. Prince, and David S. Weiss for helpful feedback. We thank Yasa Baig, Minsu Kim, Philip N. Rather, and Stuart A. West for their critical reading of an earlier version of the manuscript. This work was partially supported by grants from National Institutes of Health (LY: R01GM098642), Office of Naval Research (LY: N00014-20-1-2121), Defense Advanced Research Projects Agency (LY: 2501-203-2015861), and National Science Foundation (LY & CTL: MCB-1937259). The funders had no role in study design, data collection and analysis, decision to publish, or preparation of the manuscript.

Author contributions

E. Ş.: Conceived the study, designed, and conducted the research. Wrote the manuscript. C. A. V.: Assisted with experiments in **Figure 1** and **Supplementary Figure 8**. K. S.: Assisted with experiments in **Supplementary Figure 10**. Z. Z. Assisted with experiments in **Supplementary Figure 6**A and **Supplementary Figure 15** A. Wrote the cylindrically symmetric antibiotic gradient solution in the Supplementary Information. N. L.: Made observations that

inspired this study. D. L.: Constructed the fluorescent protein-labeled variant of *Klebsiella* (*Klebsiella*-mCherry). Assisted in the experiments that led to **Supplementary Figure 8**. H. R. M.: Assisted in the isolation of the hospital sink bacteria. D. J. A.: Obtained and provided the p-trap water samples which led to the isolation of the hospital sink bacteria. C. T. L.: Assisted with data interpretation, writing the manuscript, and articulating the broader ecological context. L. Y.: Conceived the study and assisted with research design and data interpretation. Wrote the manuscript.

All authors contributed to the reviewing and editing of manuscript drafts and approved the final version.

Conflicts of interest

None are declared.

Data availability

All data is available in the main text, the supplementary material, or will be made available upon request.

Code availability

Codes will be made available upon request.

References

1 Paine, R. T. A Note on Trophic Complexity and Community Stability. *Am Nat* **103**, 91-93, doi:10.1086/282586 (1969).

2 Power, M. E. *et al.* Challenges in the Quest for Keystones. *BioScience* **46**, 609-620, doi:10.2307/1312990 (1996).

3 Jones, C. G., Lawton, J. H. & Shachak, M. Organisms as Ecosystem Engineers. *Oikos* **69**, 373-386, doi:10.2307/3545850 (1994).

4 Hastings, A. *et al.* Ecosystem engineering in space and time. *Ecol Lett* **10**, 153-164, doi:https://doi.org/10.1111/j.1461-0248.2006.00997.x (2007).

5 Duchardt, C. J., Porensky, L. M. & Pearse, I. S. Direct and indirect effects of a keystone engineer on a shrubland-prairie food web. *Ecology* **102**, e03195, doi:https://doi.org/10.1002/ecy.3195 (2021).

6 Yeakel, J. D. *et al.* Diverse interactions and ecosystem engineering can stabilize community assembly. *Nat Commun* **11**, 3307, doi:10.1038/s41467-020-17164-x (2020).

7 Banerjee, S., Schlaeppi, K. & van der Heijden, M. G. A. Keystone taxa as drivers of microbiome structure and functioning. *Nature Reviews Microbiology* **16**, 567-576, doi:10.1038/s41579-018-0024-1 (2018).

8 Losapio, G., Genes, L., Knight, C. J., McFadden, T. N. & Pavan, L. Monitoring and modelling the effects of ecosystem engineers on ecosystem functioning. *Functional Ecology* **n/a**, doi:https://doi.org/10.1111/1365-2435.14315.

9 Harvey, E., Gounand, I., Ward, C. L. & Altermatt, F. Bridging ecology and conservation: from ecological networks to ecosystem function. *Journal of Applied Ecology* **54**, 371-379, doi:https://doi.org/10.1111/1365-2664.12769 (2017).

10 Boogert, N. J., Paterson, D. M. & Laland, K. N. The Implications of Niche Construction and Ecosystem Engineering for Conservation Biology. *BioScience* **56**, 570-578, doi:10.1641/0006-3568(2006)56[570:Tionca]2.0.Co;2 (2006).

11 Ze, X., Duncan, S. H., Louis, P. & Flint, H. J. Ruminococcus bromii is a keystone species for the degradation of resistant starch in the human colon. *ISME J* **6**, 1535-1543, doi:10.1038/ismej.2012.4 (2012).

12 Kropp, C. *et al.* The Keystone commensal bacterium Christensenella minuta DSM 22607 displays anti-inflammatory properties both in vitro and in vivo. *Sci Rep* **11**, 11494, doi:10.1038/s41598-021-90885-1 (2021).

13 Hajishengallis, G. *et al.* Low-Abundance Biofilm Species Orchestrates Inflammatory Periodontal Disease through the Commensal Microbiota and Complement. *Cell Host & Microbe* **10**, 497-506, doi:10.1016/j.chom.2011.10.006 (2011).

14 Flynn, J. M., Niccum, D., Dunitz, J. M. & Hunter, R. C. Evidence and Role for Bacterial Mucin Degradation in Cystic Fibrosis Airway Disease. *PLoS Pathog* **12**, e1005846, doi:10.1371/journal.ppat.1005846 (2016).

15 Centanni, M. *et al.* Bifidobacterium pseudolongum in the Ceca of Rats Fed Hi-Maize Starch Has Characteristics of a Keystone Species in Bifidobacterial Blooms. *Appl Environ Microbiol* **84**, e00547-00518, doi:doi:10.1128/AEM.00547-18 (2018).

16 Cartmell, A. *et al.* A surface endogalactanase in Bacteroides thetaiotaomicron confers keystone status for arabinogalactan degradation. *Nat Microbiol* **3**, 1314-1326, doi:10.1038/s41564-018-0258-8 (2018).

17 Chng, K. R. *et al.* Metagenome-wide association analysis identifies microbial determinants of post-antibiotic ecological recovery in the gut. *Nature Ecology & Evolution* **4**, 1256-1267, doi:10.1038/s41559-020-1236-0 (2020).

18 Feng, J. *et al.* Polysaccharide utilization loci in Bacteroides determine population fitness and community-level interactions. *Cell Host & Microbe* **30**, 200-215.e212, doi:10.1016/j.chom.2021.12.006 (2022).

19 Weiss, A. S. *et al.* Nutritional and host environments determine community ecology and keystone species in a synthetic gut bacterial community. *Nat Commun* **14**, 4780, doi:10.1038/s41467-023-40372-0 (2023).

20 Hajishengallis, G., Darveau, R. P. & Curtis, M. A. The keystone-pathogen hypothesis. *Nature Reviews Microbiology* **10**, 717-725, doi:10.1038/nrmicro2873 (2012).

21 Hajishengallis, G. & Lamont, R. J. Dancing with the Stars: How Choreographed Bacterial Interactions Dictate Nososymbiocity and Give Rise to Keystone Pathogens, Accessory Pathogens, and Pathobionts. *Trends Microbiol* **24**, 477-489, doi:10.1016/j.tim.2016.02.010 (2016).

22 Fenchel, T. Microbial Behavior in a Heterogeneous World. *Science* **296**, 1068-1071, doi:doi:10.1126/science.1070118 (2002).

23 Costerton, J. W., Geesey, G. G. & Cheng, K. J. How bacteria stick. *Sci Am* **238**, 86-95, doi:10.1038/scientificamerican0178-86 (1978).

24 Or, D., Smets, B. F., Wraith, J. M., Dechesne, A. & Friedman, S. P. Physical constraints affecting bacterial habitats and activity in unsaturated porous media – a review. *Advances in Water Resources* **30**, 1505-1527, doi:https://doi.org/10.1016/j.advwatres.2006.05.025 (2007).

25 Le, S. *et al.* Bacteriophage protein Dap1 regulates evasion of antiphage immunity and Pseudomonas aeruginosa virulence impacting phage therapy in mice. *Nat Microbiol*, doi:10.1038/s41564-024-01719-5 (2024).

26 Mitchell, J. G. & Kogure, K. Bacterial motility: links to the environment and a driving force for microbial physics. *FEMS Microbiology Ecology* **55**, 3-16, doi:10.1111/j.1574-6941.2005.00003.x (2006).

27 Tsao, Y.-F. *et al.* Phage Morons Play an Important Role in Pseudomonas aeruginosa Phenotypes. *J Bacteriol* **200**, 10.1128/jb.00189-00118, doi:doi:10.1128/jb.00189-18 (2018).

28 Shah, M. *et al.* A phage-encoded anti-activator inhibits quorum sensing in Pseudomonas aeruginosa. *Mol Cell* **81**, 571-583.e576, doi:https://doi.org/10.1016/j.molcel.2020.12.011 (2021).

29 Finkelshtein, A., Roth, D., Jacob, E. B. & Ingham, C. J. Bacterial Swarms Recruit Cargo Bacteria To Pave the Way in Toxic Environments. *MBio* **6**, 10.1128/mbio.00074-00015, doi:doi:10.1128/mbio.00074-15 (2015).

30 Caiazza, N. C., Shanks, R. M. Q. & O'Toole, G. A. Rhamnolipids Modulate Swarming Motility Patterns of Pseudomonas aeruginosa. *J Bacteriol* **187**, 7351-7361, doi:doi:10.1128/jb.187.21.7351-7361.2005 (2005).

31 Luo, N. *et al.* The collapse of cooperation during range expansion of Pseudomonas aeruginosa. *Nat Microbiol*, doi:10.1038/s41564-024-01627-8 (2024).

32 Meredith, H. R. *et al.* Applying ecological resistance and resilience to dissect bacterial antibiotic responses. *Science Advances* **4**, eaau1873, doi:doi:10.1126/sciadv.aau1873 (2018).

33 Magill, S. S. *et al.* Multistate Point-Prevalence Survey of Health Care–Associated Infections. *New England Journal of Medicine* **370**, 1198-1208, doi:10.1056/NEJMoa1306801 (2014).

34 Rennie, R. P., Jones, R. N. & Mutnick, A. H. Occurrence and antimicrobial susceptibility patterns of pathogens isolated from skin and soft tissue infections: report from the SENTRY Antimicrobial Surveillance Program (United States and Canada, 2000). *Diagnostic Microbiology and Infectious Disease* **45**, 287-293, doi:https://doi.org/10.1016/S0732-8893(02)00543-6 (2003).

35 Rashid, M. H. & Kornberg, A. Inorganic polyphosphate is needed for swimming, swarming, and twitching motilities of Pseudomonas aeruginosa. *Proceedings of the National Academy of Sciences* **97**, 4885-4890, doi:doi:10.1073/pnas.060030097 (2000).

36 Arslan, E., Coşkun, M. K., Çobanoğlu, Ş., Aslan, M. H. & Yazıcı, A. Effects of four antibiotics on Pseudomonas aeruginosa motility, biofilm formation, and biofilm-specific antibiotic resistance genes expression. *Diagnostic Microbiology and Infectious Disease* **106**, 115931, doi:https://doi.org/10.1016/j.diagmicrobio.2023.115931 (2023).

37 Kumar, L., Brenner, N., Brice, J., Klein-Seetharaman, J. & Sarkar, S. K. Cephalosporins Interfere With Quorum Sensing and Improve the Ability of Caenorhabditis elegans to Survive Pseudomonas aeruginosa Infection. *Front Microbiol* **12**, doi:10.3389/fmicb.2021.598498 (2021).

38 Liu, Y., Lehnert, T. & Gijs, M. A. M. Effect of inoculum size and antibiotics on bacterial traveling bands in a thin microchannel defined by optical adhesive. *Microsystems & Nanoengineering* **7**, 86, doi:10.1038/s41378-021-00309-3 (2021).

39 Oliveira, N. M. *et al.* Suicidal chemotaxis in bacteria. *Nat Commun* **13**, 7608, doi:10.1038/s41467-022-35311-4 (2022).

40 Berg, H. C. *Random Walks in Biology*
New and Expanded Edition. REV - Revised edn, (Princeton University Press, 1993).

41 Luo, N., Wang, S., Lu, J., Ouyang, X. & You, L. Collective colony growth is optimized by branching pattern formation in Pseudomonas aeruginosa. *Mol Syst Biol* **17**, e10089, doi:https://doi.org/10.15252/msb.202010089 (2021).

42 Starlander, G. & Melhus, Å. Minor outbreak of extended-spectrum β-lactamase-producing Klebsiella pneumoniae in an intensive care unit due to a contaminated sink. *Journal of Hospital Infection* **82**, 122-124, doi:https://doi.org/10.1016/j.jhin.2012.07.004 (2012).

43 Hota, S. *et al.* Outbreak of Multidrug-Resistant Pseudomonas aeruginosa Colonization and Infection Secondary to Imperfect Intensive Care Unit Room Design. *Infection Control & Hospital Epidemiology* **30**, 25-33, doi:10.1086/592700 (2009).

44 Kotay, S., Chai, W., Guilford, W., Barry, K. & Mathers, A. J. Spread from the Sink to the Patient: In Situ Study Using Green Fluorescent Protein (GFP)-Expressing Escherichia coli To Model Bacterial Dispersion from Hand-Washing Sink-Trap Reservoirs. *Appl Environ Microbiol* **83**, e03327-03316, doi:doi:10.1128/AEM.03327-16 (2017).

45 Bertness, M. D. & Callaway, R. Positive interactions in communities. *Trends Ecol Evol (Amst)* **9**, 191-193, doi:https://doi.org/10.1016/0169-5347(94)90088-4 (1994).

46 Bronstein, J. L. Conditional outcomes in mutualistic interactions. *Trends Ecol Evol (Amst)* **9**, 214-217, doi:https://doi.org/10.1016/0169-5347(94)90246-1 (1994).

47 Hoek, T. A. *et al.* Resource Availability Modulates the Cooperative and Competitive Nature of a Microbial Cross-Feeding Mutualism. *PLoS Biol* **14**, e1002540, doi:10.1371/journal.pbio.1002540 (2016).

48 Fetzer, I. *et al.* The extent of functional redundancy changes as species' roles shift in different environments. *Proceedings of the National Academy of Sciences* **112**, 14888-14893, doi:doi:10.1073/pnas.1505587112 (2015).

49 Thiery, S. & Kaimer, C. The Predation Strategy of Myxococcus xanthus. *Front Microbiol* **11**, doi:10.3389/fmicb.2020.00002 (2020).

50 Elyasi Far, B., Ahmadi, Y., Yari Khosroshahi, A. & Dilmaghani, A. Microbial Alpha-Amylase Production: Progress, Challenges and Perspectives. *Adv Pharm Bull* **10**, 350-358, doi:10.34172/apb.2020.043 (2020).

51 Jin, F., Conrad, J. C., Gibiansky, M. L. & Wong, G. C. L. Bacteria use type-IV pili to slingshot on surfaces. *Proceedings of the National Academy of Sciences* **108**, 12617-12622, doi:doi:10.1073/pnas.1105073108 (2011).

52 Mattick, J. S. Type IV Pili and Twitching Motility. *Annu Rev Microbiol* **56**, 289-314, doi:https://doi.org/10.1146/annurev.micro.56.012302.160938 (2002).

53 Fortune, G. T., Oliveira, N. M. & Goldstein, R. E. Biofilm Growth under Elastic Confinement. *Phys Rev Lett* **128**, 178102, doi:10.1103/PhysRevLett.128.178102 (2022).

54 Seminara, A. *et al.* Osmotic spreading of Bacillus subtilis biofilms driven by an extracellular matrix. *Proceedings of the National Academy of Sciences* **109**, 1116-1121, doi:doi:10.1073/pnas.1109261108 (2012).

55 Zhang, Q. *et al.* Morphogenesis and cell ordering in confined bacterial biofilms. *Proceedings of the National Academy of Sciences* **118**, e2107107118, doi:doi:10.1073/pnas.2107107118 (2021).

56 Cena, J. A. d., Zhang, J., Deng, D., Damé-Teixeira, N. & Do, T. Low-Abundant Microorganisms: The Human Microbiome's Dark Matter, a Scoping Review. *Frontiers in Cellular and Infection Microbiology* **11**, doi:10.3389/fcimb.2021.689197 (2021).

57 Xavier, J. B., Kim, W. & Foster, K. R. A molecular mechanism that stabilizes cooperative secretions in Pseudomonas aeruginosa. *Mol Microbiol* **79**, 166-179, doi:10.1111/j.1365-2958.2010.07436.x (2011).

58 Fournet-Fayard, S., Joly, B. & Forestier, C. Transformation of wild type Klebsiella pneumoniae with plasmid DNA by electroporation. *J Microbiol Methods* **24**, 49-54, doi:https://doi.org/10.1016/0167-7012(95)00053-4 (1995).

59 Payne, S. *et al.* Temporal control of self-organized pattern formation without morphogen gradients in bacteria. *Mol Syst Biol* **9**, 697, doi:10.1038/msb.2013.55 (2013).

60 Barbier, M. & Damron, F. H. Rainbow Vectors for Broad-Range Bacterial Fluorescence Labeling. *PLoS ONE* **11**, e0146827, doi:10.1371/journal.pone.0146827 (2016).

61 Santos-Moreno, J., Tasiudi, E., Stelling, J. & Schaerli, Y. Multistable and dynamic CRISPRi-based synthetic circuits. *Nat Commun* **11**, 2746, doi:10.1038/s41467-020-16574-1 (2020).

62 Warren, B. G. *et al.* Identification of carbapenem-resistant organism (CRO) contamination of in-room sinks in intensive care units in a new hospital bed tower. *Infection Control & Hospital Epidemiology* **45**, 302-309, doi:10.1017/ice.2023.289 (2024).